Arch. Metall. Mater. **62** (2017), 2, 841-849

DOI: 10.1515/amm-2017-0124

A. TRENCZEK-ZAJĄC*#, J. BANAŚ*, K. ŚWIERCZEK**, K. ZAZAKOWNY*, M. RADECKA*

PHOTOSENSITIZATION OF TiO_2 P25 WITH CdS NANOPARTICLES FOR PHOTOCATALYTIC APPLICATIONS

A TiO_2/CdS coupled system was prepared by mixing the TiO_2 P25 with CdS synthesized by means of the precipitation method. It was found that the specific surface area (SSA) of both components is extremely different and equals 49.5 for TiO_2 and 145.4 $m^2 \cdot g^{-1}$ for CdS. The comparison of particle size distribution and images obtained by means of transmission electron microscopy (TEM) showed agglomeration of nanocomposites. X-ray diffraction (XRD) patterns suggest that CdS crystallizes in a mixture of cubic and hexagonal phases. Optical reflectance spectra revealed a gradual shift of the fundamental absorption edge towards longer wavelengths with increasing CdS molar fraction, which indicates an extension of the absorption spectrum of TiO_2. The photocatalytic activity in UV and UV-vis was tested with the use of methyl orange (MO). The Langmuir–Hinshelwood model described well the photodegradation process of MO. The results showed that the photocatalytic behaviour of the TiO_2/CdS mixture is significantly better than that of pure nanopowders.

Keywords: semiconductors, X-ray diffraction, transmission electron microscopy (TEM), catalytic properties, optical properties

1. Introduction

Nanocomposites are defined as a mixture of two immiscible materials of which at least one has nanoscale dimensions. The constituents of nanocomposites exhibit different structures, composition, and properties. Such materials are generally used when a combination of properties is required that cannot be found in a single material. Differences in the electronic structure of nanocomposites based on metal oxides/sulphides have a profound influence on photocatalytic properties. The mixture of semiconductors based on TiO_2/CdS has attracted attention because of their potential applications in the photodegradation of organic pollutants [1-16], the photoelectrolysis of water for hydrogen production [17-20], and the sensitization of solar cells [21,22]. Due to its wide band gap (3.0 for rutile and 3.2 eV for anatase), TiO_2 is able to absorb light in the UV range, which constitutes 3-5% of solar irradiation, while semiconductors with a narrower band gap, such as CdS, are effective under visible light. With a band gap of 2.5 eV, CdS used to sensitize TiO_2 is an efficient way to obtain catalysts with extended absorption of visible light and higher photocatalytic efficiency. The energy band edge positions of semiconductors in composites are also important parameters. The behaviour of a semiconductor junction depends to a very large degree on the alignment of the energy bands at the interface. For CdS/TiO_2 coupling, the type I heterostructures are formed [23]. The conduction band of CdS is higher than that of TiO_2 (see Table 1); the electrons originating from cadmium sulphide can be injected into titanium dioxide via irradiation with visible light [4]. This process promotes the separation of electron-hole pairs. Numerous reports on the development of composites comprising a CdS bulk with TiO_2 particles have been presented.

TABLE 1

Band positions of TiO_2 and CdS in an aqueous solution [4]. V *vs* NHE – potential versus normal hydrogen electrode

Semiconductor	Valence band (V vs NHE)	Conduction band (V vs NHE)	Band gap (eV)
TiO_2 anatase	+3.1	–0.1	3.2
CdS	+2.1	–0.4	2.5

It is known that the bulk nature may reduce the ability of CdS to be coupled with TiO_2, adversely affecting the photosensitization of TiO_2 with CdS for photocatalysis [24]. The architecture of the elements of a nanocomposite material is critical. Several strategies for the creation of the coupling system have been proposed [25]. The components of a composite can be built from elementary units such as nanoparticles (0D), molecular chains, corals, fibres, nanotubes (1D), thin films, or plates (2D). The last group (3D) is not confined to the nanoscale in any dimension. It is an interconnected system composed of a variety of forms.

* AGH UNIVERSITY OF SCIENCE AND TECHNOLOGY, FACULTY OF MATERIALS SCIENCE AND CERAMICS, DEPARTMENT OF INORGANIC CHEMISTRY, AL. A. MICKIEWICZA 30, 30-059 KRAKOW, POLAND
** AGH UNIVERSITY OF SCIENCE AND TECHNOLOGY, FACULTY OF ENERGY AND FUELS, DEPARTMENT OF HYDROGEN ENERGY, AL. A. MICKIEWICZA 30, 30-059 KRAKOW, POLAND
# Corresponding author: anita.trenczek-zajac@agh.edu.pl

The main features of a nanostructure ideal for photocatalysis include:

- sufficiently large surface area (a sufficiently high number of active sites)
- light absorption in the UV-vis range
- effective separation of photo-induced electronic charge carriers
- the nanostructure should contain a TiO_2 component in one of the four above-mentioned forms (0D, 1D, 2D or 3D).

Four types of a coupling system used to sensitize TiO_2 with CdS are therefore possible for CdS in the 0D form.

Our earlier studies of a TiO_2/CdS coupled system [20] consisting of titanium dioxide flower-like nanostructures (3D) decorated with CdS/PbS nanoparticles (0D) focused on the influence of CdS and PbS quantum dots on the optical and photoelectrochemical behaviour of titanium dioxide nanoflowers. It was concluded that the modification of a photoanode based on TiO_2 via the deposition of QDs-CdS improves current–voltage characteristics of photoelectrochemical cells, both for white light and for the vis region.

The efficiency of photocatalytic reactions depends on the composition of TiO_2/CdS [6]. On the other hand, certain types of TiO_2 template can protect CdS from photodegradation [3]. Usually, application of cadmium sulfide is limited due to its photocorrosion by the photogenerated holes [6]. Therefore, in this work, systematically studies of TiO_2-CdS system in the form of nanocomposites are performed. Full composition range extending from 100 mol% TiO_2 to 100 mol% CdS was covered.

The aim of the presented research was to study the morphological properties as well as the performance of TiO_2/CdS nanocomposites during the photodegradation of methyl orange. The intentional mixing of constituents of different size was considered as a possibility of improving microstructure and, subsequently, the photocatalytic properties. Nanoparticles of cadmium sulphide (featuring a crystallite size of about 3 nm) used to sensitize the TiO_2 P25 nanopowder were studied. Evonik's titanium dioxide P25 nanopowder is often recognized as a standard in photocatalysis [26]. It is a bi-phase of TiO_2 (80 wt% anatase and 20 wt% rutile) nanoparticles with a crystallite size of 25-40 nm.

2. Experimental

2.1. TiO_2/CdS nanocomposite preparation

TiO_2/CdS coupled systems with the composition varying from 100 mol% TiO_2 to 100 mol% CdS were prepared from commercial TiO_2 P25 nanopowder (Evonik Degussa) – a mixture of anatase and rutile – and CdS nanopowder synthesized via the precipitation method. To precipitate cadmium sulphide, two separate solutions with a concentration of 0.1 M were obtained using distilled water: a cadmium nitrate solution was prepared by dissolving $Cd(NO_3)_2 \cdot 4H_2O$ (99+%, Acros), and a sodium sulphide one was prepared by dissolving $Na_2S \cdot 9H_2O$ (≥98.0%, Sigma Aldrich). The two solutions were then mixed, and a precipitate was rinsed and filtered with the use of a Büchner funnel. The filtered powder was subsequently dried. Afterwards, in order to obtain a full range of composition between 100% TiO_2 and 100% CdS, appropriate amounts of nanopowders were mixed via milling with zirconia balls in ethanol in a planetary mill (Fritsch, Pulverisette 6) for 1h and then drying.

2.2. Experimental methods

In order to determine the various properties of TiO_2/CdS nanocomposites, the following methods were used: transmission electron microscopy (TEM), Brunauer-Emmett-Teller adsorption isotherms (BET), dynamic light scattering technique (DLS), X-ray diffraction (XRD), spectrophotometry, and photocatalytic decomposition of organic pollutants.

TEM images were obtained using a JOEL-JEM1011 transmission electron microscope. The ImageJ software was used to evaluate the grain size of the nanopowders [27]. The specific surface area (SSA) was determined from Brunauer-Emmett-Teller (BET) nitrogen adsorption isotherms obtained with the Nova 1200e (Quantachrome). SSA, defined as the total surface area per unit of mass, was used to calculate the nanoparticles' diameter under the assumption that the samples exhibit nonporous, monodisperse and spherical morphology. In this case, SSA can be expressed by the formula (1):

$$r_{avg} = 3 / SSA \times \sum \left(x_i \times \rho_i \right) \tag{1}$$

where x is the volume ratio of each phase, ρ denotes density, and i is the appropriate phase.

Particle size distribution of nanocomposites dispersed in ethanol was determined with a Nanosizer-ZS (Malvern Instruments), on the basis of Brownian motion, using the dynamic light scattering technique (DLS). The phase analysis was carried out based on the X-ray diffraction data acquired with an X'Pert Pro diffractometer (PANalitycal) with Kα1 = 1.5406 Å, in the angular range of 20-80°. Phase identification was performed with the use of the X'Pert HighScore Plus software and the PDF database, while crystallite size was calculated from the Scherrer equation [28]. The spectral dependence of the diffused reflectance spectrum was measured over a wide wavelength (λ) range of 250-2500 nm with a Lambda 19 Perkin-Elmer double beam spectrophotometer equipped with a 150-mm integrating sphere.

The photocatalytic activity of TiO_2/CdS nanopowders was tested through the decomposition of methyl orange (MO), which is a notable example of an azo dye, and served as an organic contaminant. Photodegradation tests were carried out in a cylindrical photoreactor comprising six 8W UV (365 nm peak) or UV-vis lamps for ultraviolet and visible irradiation, respectively, and a quartz beaker which served as the reaction vessel. The distance between quartz beaker and the lamps was 8 cm. The concentration of the water-based solution of MO was $5 \cdot 10^{-5}$ M. The photocatalyst concentration in the reaction vessel was 0.625 mg $\cdot$ cm^{-3}. The mixture was continuously stirred magnetically throughout the process. For each measurement during

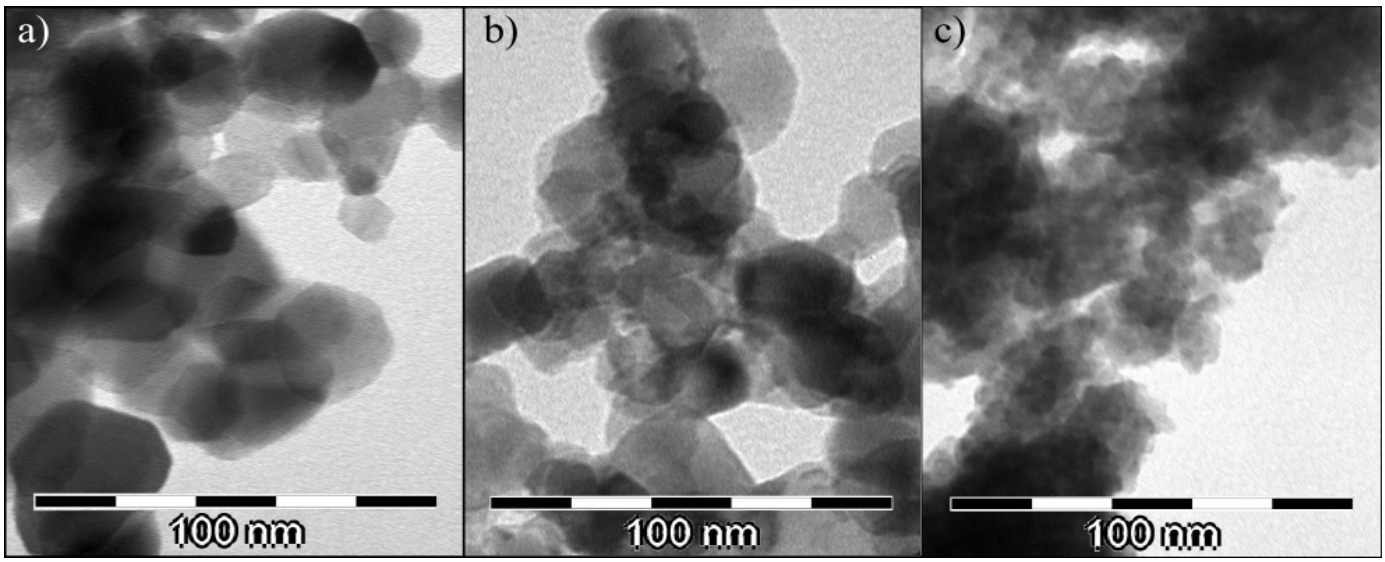

Fig. 1. TEM images of 0C (a), 50C (b) and 100C (c) nanopowders

the photocatalytic test, 5 cm^3 of the mixture was extracted from the reaction vessel, filtered and analyzed with the use of Vis-7220G Single Beam Spectrophotometer (Biotech Engineering Management Co. Ltd.). The measurement of maximum absorbance was performed for 464 nm.

3. Results and discussion

TEM images of nanocomposites are presented in Fig. 1. In the case of pure titanium dioxide (the 0C powder), the images show oval grains with a size of 12-40 nm (Fig. 1a). The pure CdS (100C) powder is significantly agglomerated; however, small grains (2-12 nm) are pronounced (Fig. 1c). For a mixture of powders (50C) smaller particles of CdS can clearly be distinguished between TiO_2 grains (Fig. 1b).

Fig. 2 shows the specific surface area (SSA) as well as the corresponding particle size calculated from BET using eq. 1; both of these properties are presented as a function of composition. As can be seen, pure TiO_2 and CdS nanopowders exhibit different specific surface areas of SSA = 49.5 $m^2 \cdot g^{-1}$ (TiO_2) and SSA = 145.4 $m^2 \cdot g^{-1}$ (CdS), which correspond to BET – equivalent particle diameters equal to 30.8 nm and 8.5 nm in the case of TiO_2 and CdS, respectively. The addition of CdS results in an almost linear growth of the specific surface area up to 114 $m^2 \cdot g^{-1}$ for 50 mol% of CdS. A further increase in the CdS concentration leads to a continued rise, which, however, is somewhat less significant. Particle size calculated from BET changes over a wide range. Even a small addition of cadmium sulphide to titanium dioxide causes a rapid decrease in particle size. Nanocomposites with 25 mol% of CdS are characterized by particles that are about half the size of TiO_2 – 16 and 31 nm, respectively. Grains of cadmium sulphide, however, are as small as 8 nm. These results are highly consistent with those obtained from the analysis based on TEM images. The detailed results of the BET analysis are collected in Table 2.

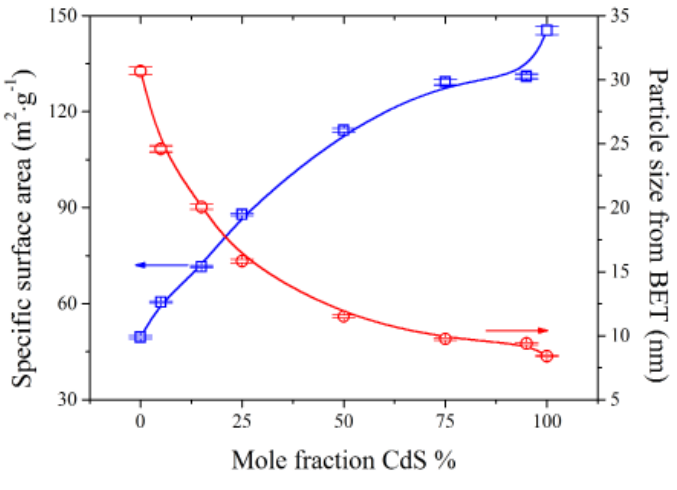

Fig. 2. Specific surface area and particle size of nanocomposites

TABLE 2

Detailed data on the composition of TiO_2/CdS nanocomposites and the results of BET analysis

Name	Mole fraction (%)		Specific surface area ($m^2 \cdot g^{-1}$)	Grain size from BET (nm)	Particle size distribution by volume	
	CdS	TiO_2			Fraction (%)	Mean (µm)
0C	0	100	49.5 ±0.4	30.8 ±0.3	10.1	0.16
					5.6	0.55
					7.7	5.30
5C	5	95	60.5 ±0.2	24.6 ±0.2	17.3	0.13
15C	15	85	71.5 ±0.3	20.1 ±0.2	19.3	0.14
25C	25	75	87.9 ±0.3	16.4 ±0.2	19.0	2.06
50C	50	50	114.2 ±0.5	12.0 ±0.1	5.8	1.42
					19.7	5.42
75C	75	25	129.3 ±1.0	10.1 ±0.1	9.8	2.17
					9.4	5.47
95C	95	5	131.0 ±0.7	9.4 ±0.1	2.9	0.13
					2.7	0.61
					26.9	5.45
100C	100	0	145.4 ±1.3	8.5 ±0.1	2.9	1.90
					27.3	5.32

The intensity, volume, and numerical distribution of particle size for 0C, 50C and 100C nanocomposites are presented in Fig. 3. Mean values as an "average" of particle size distribution by volume for all TiO_2-CdS nanopowders are collected in Table 2. The analysis of the distribution of particle diameter of TiO_2/CdS shows that more than 10% of 0C particles have mean volume fraction (mvf) equal to 0.16 μm. There is also a negligible number of particles with an mvf of 0.55 and 5.30 μm. In the case of 100C, more than 27% of particles have an mvf of 5.32 μm. The lowest volume fraction with a mean of 1.9 μm is insignificant in number. The 50C nanocomposite is composed of two main fractions of particles: one with a prevalence of about 6% and an mvf equal to 1.42 μm, and another one, which constitutes 20% and exhibits an mvf of 5.42 μm. It can also be noticed that the intensity and volume fraction dependences of 50C and 100C are to a large degree similar. Based on the comparison of particle size calculated from BET, TEM images and particle size distribution, it can be noted that all nanocomposites are agglomerated.

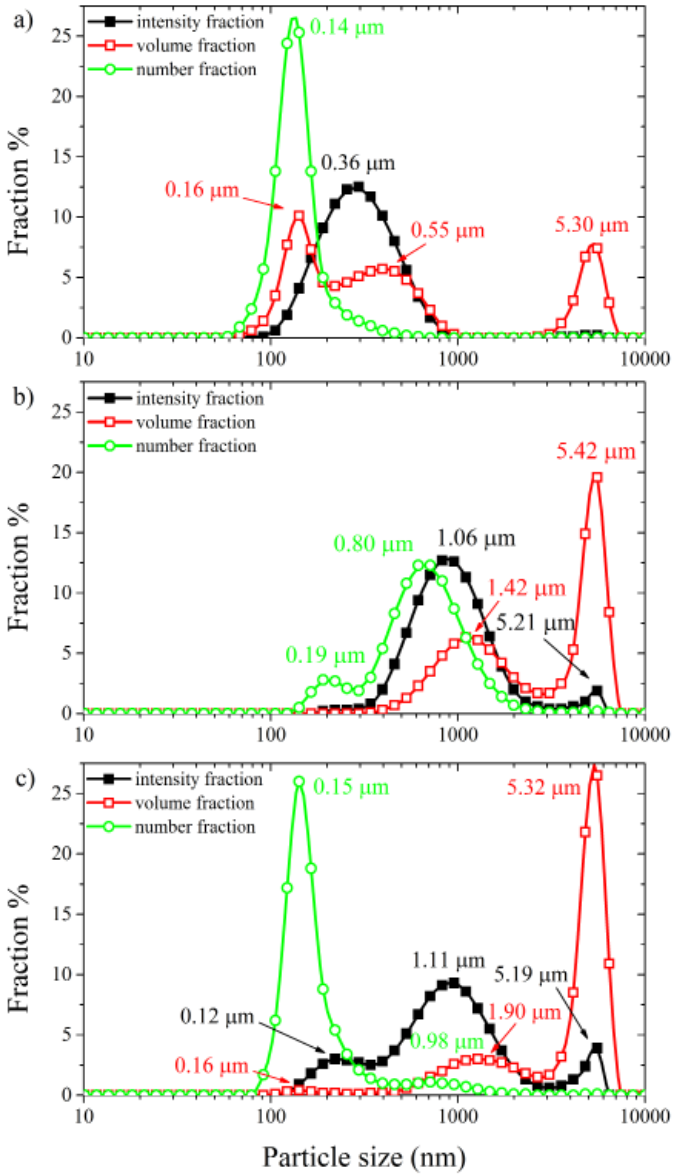

Fig. 3. Distribution of particle diameter of TiO_2/CdS nanocomposites by intensity, volume and number for 0C (a), 50C (b) and 100C (c)

The evolution of X-ray diffraction patterns upon changing the composition from 100 mol% TiO_2 to 100 mol% CdS is presented in Fig. 4. As expected, it was found that the 0C powder is composed of tetragonal anatase (JCPDS-ICDD #00-021-1272) (~80%) and rutile (JCPDS-ICDD #00-021-1276) (~20%) TiO_2 phases. In the case of 100C, the peak width at half-height is very high, which leads to peak overlap. A similar diffraction pattern was observed for CdS nanopowder by White et al. [29], and assigned to cubic polymorph. However, a careful analysis of the 2θ range between 39-60° reveals an increase in the intensity between peaks at 44.1° and 52.2°; this can be ascribed to the hexagonal (103) position (JCPDS-ICDD #00-041-1049). Thus, the possibility of the coexistence of poorly crystallized cubic (JCPDS-ICDD #01-075-0581) and hexagonal phases with a certain amount of an amorphous component cannot be excluded. The addition of CdS to TiO_2 or vice versa leads to a clear mixture – the X-ray diffraction pattern reveals the presence of both phases. The size of CdS crystallites is several times smaller than that of TiO_2 – ~3 nm for cadmium sulphide, 25 nm for anatase, and 41 nm for rutile.

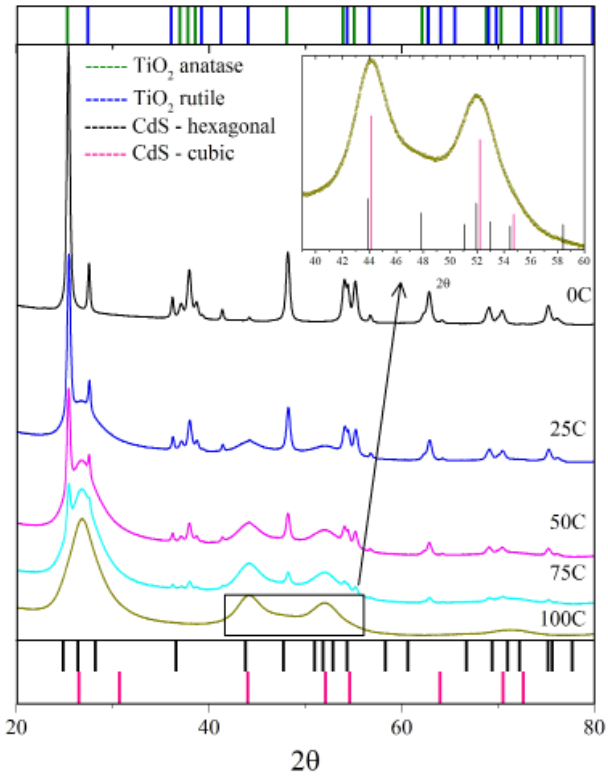

Fig. 4. X-ray diffraction patterns of TiO_2/CdS nanopowders. Inset: 2θ range between 39-60°

In order to study the electronic structure of TiO_2/CdS nanocomposites, optical spectrometry UV-vis measurements were performed. Fig. 5 presents the optical reflectance spectra $R_{total}(\lambda)$ obtained for nanopowders with different molar contribution of pure TiO_2 and CdS. The absorption edge is observed between 300 and 400 nm for TiO_2, and between 500 and 650 nm for CdS. As can be seen, there is a gradual shift of the fundamental absorption edge towards longer wavelength with increasing

CdS molar fraction. Changes in reflectance occur simultaneously with changes in the colour of the powder – from white for TiO_2 to intense orange for CdS. Interestingly, the addition of as little as 5 mol% of CdS to the TiO_2 nanopowder results in a drastic modification of the reflection spectrum in the visible region of light between 400 and 500 nm. In a comparison with TiO_2 and CdS, a transition region is demonstrated by a change in the value of reflectance, which reaches 45% in comparison with 100% for 0C and 5% for 100C nanopowders. Similarly, the greatest change in the specific surface area is also observed for the 5C nanocomposite. The increase in the concentration of CdS is accompanied by corresponding changes in the reflection coefficient. The shape of the curve of nanocomposites indicates fundamental absorption edges of both components: TiO_2 and CdS. A similar spectral dependence was observed by Y. Bessekhouad et al. [3] for the CdS/TiO_2 coupled system prepared by means of the sol-gel method, via the precipitation of TiO_2 on CdS.

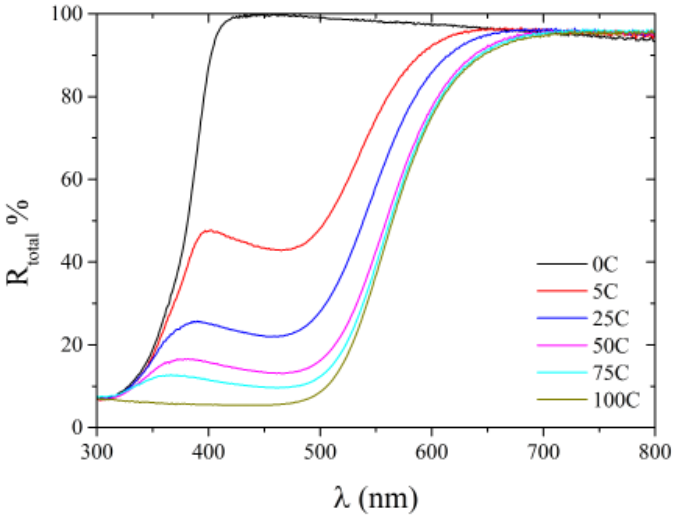

Fig. 5. Reflectance spectra of TiO_2/CdS nanopowders

Based on the reflectance spectra presented in Fig. 5, the band gap energies (E_g) of semiconductors were calculated. For this purpose, the Kubelka-Munk model was used, which is expressed as the *K-M* function (2) [30]:

$$K_M\left(R_\infty\right)=\left(1-R_\infty\right)^2/\left(2\times R_\infty\right)=k/s \qquad (2)$$

where R_∞ is absolute reflectance of the sample, k is related with absolute absorption, and s is due scattering.

The extrapolation of the plot of $(K\text{-}M\cdot h\nu)^{1/n}$ (n can equal 1/2, 3/2, 2 or 3 depending on the type of band gap transition) versus ($h\nu$) to the energy axis allows the E_g value to be calculated. The band gap energy of titanium dioxide was found to be 3.51 eV for anatase and 3.38 eV for rutile; in the case of cadmium sulphide it was equal to 2.34 eV.

The photocatalytic activity of the nanocomposites was evaluated by decomposing methyl orange (MO) which is an example of an organic pollutant. Fig. 6 demonstrates the typical time-dependent UV absorption spectra of MO in the presence of a photocatalyst in the dark and during UV irradiation. Before exposure to light, the dye was given 10 min to let it be adsorbed on the surface of the nanocatalyst. The concentration of the dye after that time was taken as a starting point for subsequent calculations. The spectrum maximum peak for MO at 464 nm gradually decreased until it degraded completely and shifted towards blue.

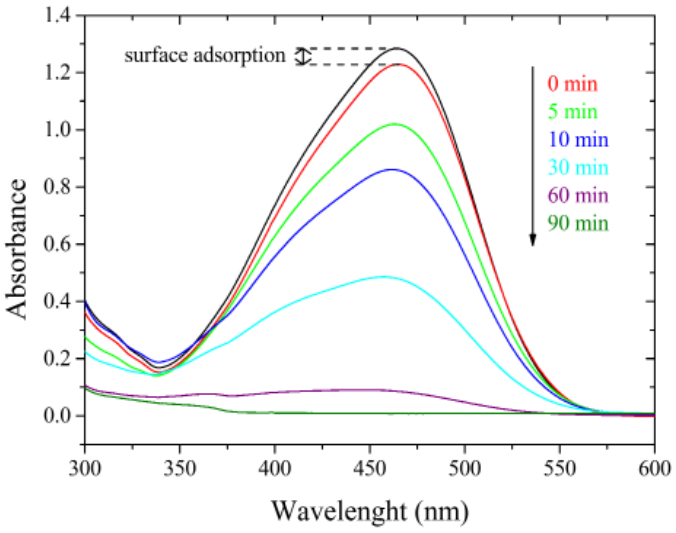

Fig. 6. Evolution of the optical absorbance peak of methyl orange in the presence of a catalyst and during UV irradiation

Fig. 7 shows the kinetics of the photocatalytic decomposition of MO as a function of irradiation time with UV and UV-vis light. To test the stability of MO in the presence of TiO_2/CdS nanocatalyst without illumination, a blank test was conducted. An appropriate amount of 0C was added to methyl orange and was stirred continuously in the dark for a long period of time.

The time needed to complete the decomposition of MO in UV light in the case of titanium dioxide is about 80 min. With increasing concentration of CdS in the nanocomposite, the degradation time increases to more than 300 min for 95C and 100C. The change in the light source from UV to UV-vis makes the photocatalytic behaviour of both the TiO_2 and the CdS (0C and 100C) nanopowders much worse than that of any of the nanocomposites in UV light; however, CdS yields a slightly better photocatalytic response. The successive addition of cadmium sulphide to titanium dioxide significantly reduces the time that is needed to decay methyl orange. The best photocatalytic activity is observed for 95 mol% of CdS (95C).

To compare the photocatalytic activity of TiO_2/CdS nanocomposites, the Langmuir-Hinshelwood model was applied to calculate the photocatalytic rates of MO decomposition, which follows the kinetic expression (3):

$$r=\frac{-dC}{dt}=\frac{k_r\cdot K\cdot C}{1+\left(K\cdot C\right)} \qquad (3)$$

where r represents the rate of photodegradation, C is the concentration of the reactant, t is irradiation time, k_r stands for the rate constant of the reaction, and K is the adsorption coefficient of the reactant.

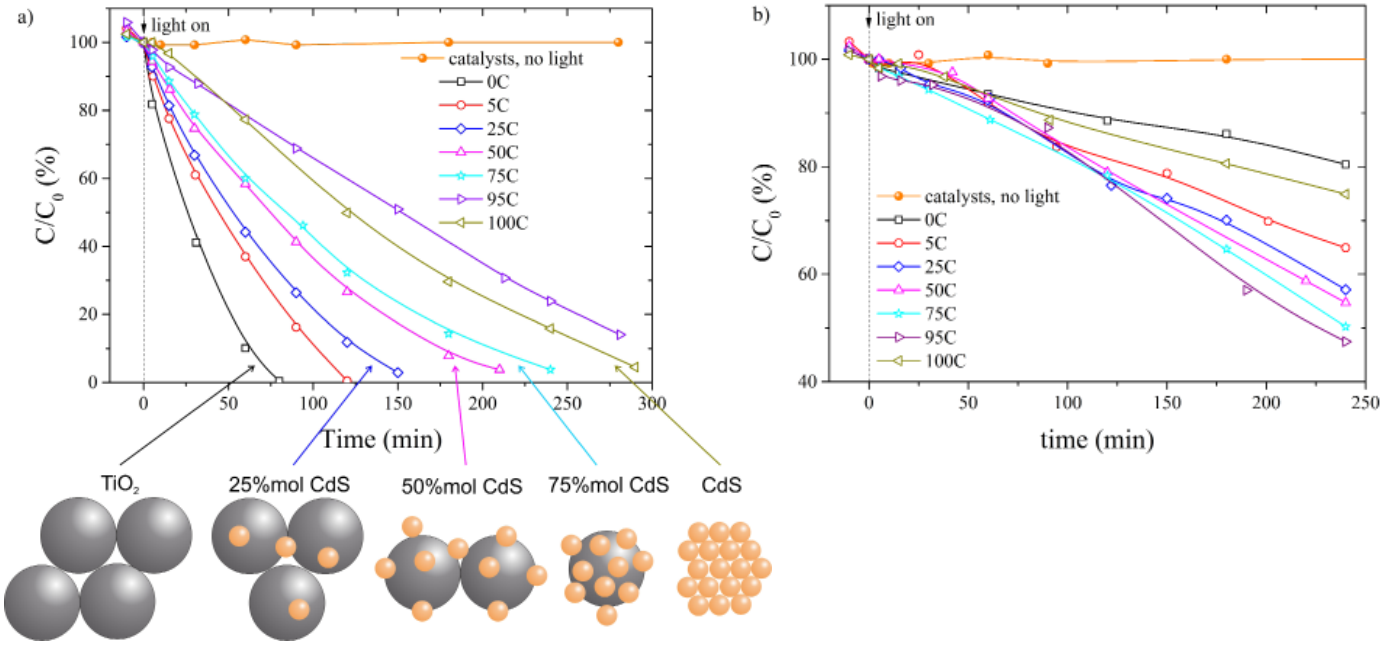

Fig. 7. Degradation of MO in the presence and absence of light, under UV light (a) and UV-vis (b)

When the initial concentration of the pollutant is sufficiently low ($C_0 < 10^{-3}$ M), the Langmuir-Hinshelwood model can be simplified to an apparent pseudo-first-order kinetics (4):

$$\ln\left(\frac{C_0}{C}\right) = k \cdot K \cdot t = k_{app} t \tag{4}$$

where k_{app} is the apparent pseudo-first-order reaction rate constant (min^{-1}).

The plot of $-\ln(C/C_0)$ as a function of time (t) may be represented with a straight line where the slope is equal to the apparent first-order rate constant k_{app}. The value of k_{app} indicates the photocatalytic activity of the photocatalyst.

Fig. 8 shows the kinetics and linear fits of $-\ln(C/C_0)$ against time. The value of k_{app} for the decomposition of MO in UV light, obtained from the linear regression analysis of data presented in Fig. 7 with the use of eq. (4), varies between $3.37 \cdot 10^{-2}$ for 0C and $5.5 \cdot 10^{-3}$ min^{-1} for 95C. In the case of UV-vis light irradiation, k_{app} varies between $0.9 \cdot 10^{-3}$ and $3.1 \cdot 10^{-3}$ min^{-1} for 0C and 95C, respectively. The results of k_{app} calculations involving the correlation coefficient R^2 are collected in Table 3.

The dependence between the chemical composition of the coupled system and the apparent pseudo-first-order reaction rate constant is presented in Fig. 9. When UV light is used, there is a strong influence of the addition of CdS to TiO_2 – the higher the concentration of CdS, the lower the values of k_{app}. This effect can be explained on the basis of changes in the interface between TiO_2 and CdS nanoparticles which occurs during incensement of the amount of CdS in the nanocomposite. First of all, the growth of the amount of cadmium sulfide is accompanied by a decrease of the amount of titanium dioxide. Thus, there is a gradual limita-

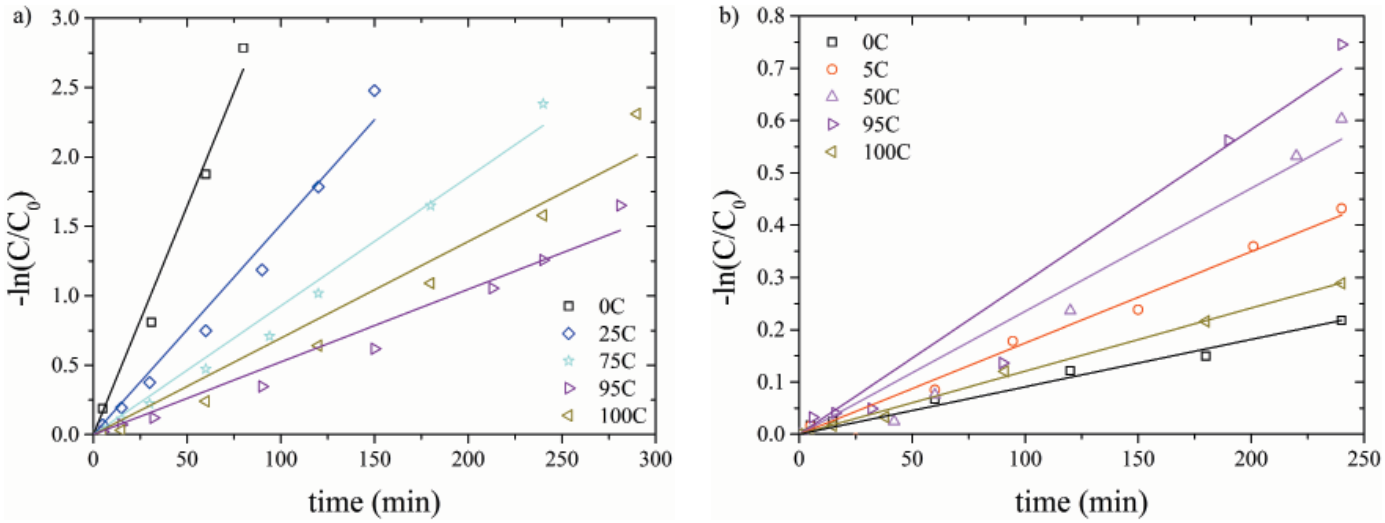

Fig. 8. First-order kinetics of methyl orange degradation using TiO_2 and CdS nanoparticles and TiO_2/CdS nanocomposites as the catalyst under UV (a) and UV-vis (b) irradiation

TABLE 3

Results and kinetic parameters of MO decomposition using TiO_2/CdS nanocomposites in UV and UV-vis light

Name	% of decomposed MO		UV		UV-vis	
	in UV after 80 min	in UV-vis after 240 min	$k \cdot 10^{-2}$ (min^{-1})	R^2	$k \cdot 10^{-3}$ (min^{-1})	R^2
0C	99.7	19.6	3.37 ±0.22	0.98	0.9 ±0.1	0.99
5C	76.5	35.1	2.14 ±0.21	0.95	1.8 ±0.1	0.98
15C	73.3	41.1	2.18 ±0.20	0.95	2.3 ±0.1	0.99
25C	67.5	42.9	1.58 ±0.08	0.98	2.3 ±0.1	0.98
50C	52.9	45.3	1.13 ±0.04	0.99	2.6 ±0.2	0.98
75C	48.3	49.8	0.97 ±0.04	0.99	2.7 ±0.2	0.97
95C	27.7	52.6	0.55 ±0.03	0.97	3.1 ±0.2	0.96
100C	32.0	25.1	0.75 ±0.05	0.97	1.2 ±0.1	1.00

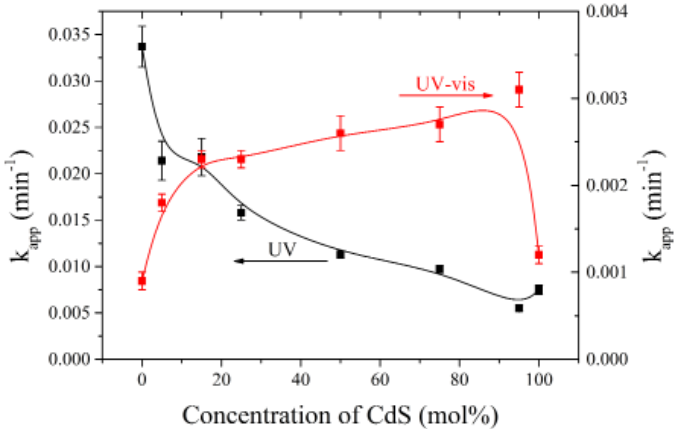

Fig. 9. The calculated apparent first-order photocatalytic degradation kinetic rate constant in the UV and UV-vis light irradiation as a function of CdS concentration in TiO_2/CdS nanocomposites

tion of the number of UV-active sites connected directly with the surface of TiO_2. Secondly, surface of TiO_2 is stepwise covered with visible-active CdS which additionally limits UV-activity. As a result, a decrease of photocatalytic activity is observed. For irradiation with UV-vis light, the improvement of the kinetics of the degradation for the TiO_2/CdS mixture is well pronounced in comparison with nanopowders composed of pure CdS and TiO_2. However, the changes induced by increasing the amount of CdS do are not as significant as those observed for UV light irradiation.

All TiO_2/CdS samples exhibit more desirable photocatalytic activity in visible light when compared to pure TiO_2 and CdS. These improved photocatalytic properties of the coupled semiconductors are related to efficient charge transport between TiO_2 and CdS as well as the morphology of the particles, and shape, size and surface contact between particles [3,5]. CdS particles loaded on TiO_2 can act as the separation centres of photoinduced charges, electrons and holes. The 95C nanocomposite in particular, with its good dispersion and the critical amount of CdS, exhibits the best performance with regard to the photodecomposition of MO.

Table 4 shows the summary of the results reported in this work and in the literature on the photodegradation of methyl orange in the presence of various TiO_2/CdS nanocomposites. The band gap energy of CdS was also placed in the table. The analysis of the data indicates that, depending on the light range, the photodegradation of 50% of methyl orange takes: 30-330 min for visible light, 7-44 min for UV light, and 45-225 min for UV-vis light. It is, however, difficult to compare the presented data directly, since among the reaction conditions there are at least three variables that affect the rate of the decomposition: the amount (0.17-1.00 $mg \cdot cm^{-3}$) or area (0.16-4.00 cm^2) of the catalyst, the concentration of MO (5-50 $mg \cdot dm^{-3}$), and the power of the light source (11-500 W). Additionally, increasing the amount or area of photocatalyst [31] and the power of light used for illumination [32], and decreasing the concentration of the dye [13,31] all lead to higher rate of decomposition.

4. Conclusion

A TiO_2/CdS mixture with the full compositional range varying from 100 mol% TiO_2 to 100 mol% CdS was prepared from pure nanopowders, commercially available TiO_2 P25 nanopowder and CdS nanopowder obtained via the precipitation method. The nanocomposites consisted of small grains and exhibited a large SSA, which changed from 145.4 $m^2 \cdot g^{-1}$ for CdS to 49.5 $m^2 \cdot g^{-1}$ for titanium dioxide. The sensitization of P25 with CdS nanoparticles extends the absorption spectrum of the TiO_2 significantly into the visible region, up to 520 nm. The photocatalytic behaviour of both the TiO_2 and the CdS nanopowders in the UV-vis light was much worse than that of any of the nanocomposites. It was demonstrated that even a small amount of CdS (5 mol%) or TiO_2 (5 mol%) in the nanocomposite improves the photocatalytic properties. A comparison of the photocatalytic activity of TiO_2/CdS nanocomposites was done based on the Langmuir-Hinshelwood model simplified to an apparent pseudo-first-order kinetics. The value of k_{app} for the decomposition of methyl orange in UV-vis light was calculated to be $0.9 \cdot 10^{-3}$ for TiO_2 and $1.2 \cdot 10^{-3}$ min^{-1} for CdS. The fastest degradation rate $3.1 \cdot 10^{-3}$ min^{-1} for 95C, which proofs considerable improvement of the photocatalytic behaviour of TiO_2/CdS heterojunction in comparison with pure nanopowders, was observed. This sensitization can be explained by the electron transfer from CdS grains to TiO_2 and the extended absorption of visible light. The highest photocatalytic activity under exposure to UV-vis light was obtained for the composition of 5 mol% TiO_2 and 95 mol% CdS.

Acknowledgments

This work was supported by the National Science Centre (NCN) based on decision no. DEC-2011/01/D/ST5/05859.

TABLE 4

Summary of reported results on the photodegradation of MO by different TiO_2/CdS nanocomposites and band gap energy of CdS. CBD – Chemical Bath Deposition, SILAR – Successive Ionic Layer Adsorption and Reaction, H-TiO_2 – hydrogenated TiO_2 (black TiO_2)

Catalyst	Reaction conditions	Time required for complete/partial degradation/rate constant	CdS band gap energy (eV)	Ref.
TiO_2/CdS heterostructure (solvothermal method)	1 mg·cm^{-3} of catalyst dispersed in MO aqueous solution (10 mg·dm^{-3}), irradiation with 300 W Xenon lamp	50% after 30 min, 95% after 120 min (visible light)	—	[7]
TiO_2 nanotubes/CdS nanoparticles (electrochemical oxidation/CBD)	4 cm^2 of catalyst immersed in 12 cm^3 of MO aqueous solution (10 mg·dm^{-3}) with addition of Na_2S and Na_2SO_3, 250 W metal halogen lamp	50% after 33 min, 96% after 180 min (visible light)	—	[8]
TiO_2 nanotubes/CdS QDs heterostructures	2.5 cm^2 of catalyst immersed in 3 cm^3 of MO aqueous solution (5 mg·dm^{-3}), 300 W Xenon lamp	50% after 120 min, 95% after 300 min (visible light)	2.34	[9]
TiO_2/CdS nanocomposites (microwave-assisted hydrothermal synthesis/CBD)	0.17 mg·cm^{-3}of catalyst dispersed in MO aqueous solution (50 mg·dm^{-3}), 125 W Mercury lamp (UV) and 1000 W Xenon lamp (sunlight simulator)	50% after 7 min, 95% after 30 min (UV light), $k_{app} = 1.25 \cdot 10^{-2}$ min^{-1}	2.09-2.21	[10]
CdS nanocrystals/TiO_2/ crosslinked chitosan composite	0.5 mg·cm^{-3}of catalyst dispersed in MO aqueous solution (15 mg·dm^{-3}), 300 W Xenon lamp	50% after 45 min, 99% after 210 min (UV-vis)	—	[11]
TiO_2 nanospheres/CdS hybrid (solvothermal process)	0.21 mg·cm^{-3}of catalyst dispersed in MO aqueous solution (10 mg·dm^{-3}), 300 W Xenon lamp	50% after 330 min, 70% after 540 min (visible light), $k_{app} = 2.2 \cdot 10^{-3}$ min^{-1}	2.3	[12]
TiO_2 nanotubes/CdS (CBD)	catalyst immersed in MO aqueous solution (16 mg·dm^{-3}), 11 W lamp (UV light), 300 W Xenon lamp (visible light)	50% after 56 min, 64% after 180 min (visible light)	—	[13]
		50% after 28 min, 99% after 120 min (UV light, PEC assisted), $k_{app} = 4.0 \cdot 10^{-2}$ min^{-1}		
		50% after 55 min, 99% after 190 min (visible light, PEC assisted), $k_{app} = 2.7 \cdot 10^{-2}$ min^{-1},		
TiO_2 nanotubes/CdS (SILAR)	2 cm^2 of catalyst immersed in 15 cm^3 of MO aqueous solution with addition of Na_2S and Na_2SO_3, 500 W Xenon lamp	50% after 160 min, 80% after 360 min (visible light)	2.32	[14]
TiO_2/CdS (sol-gel, spin coating)	MO aqueous solution (12 mg·dm^{-3})	50% after 300 min (visible light)	—	[15]
H-TiO_2/CdS heterojunction (electrodeposition of CdS)	0.16 cm^2 of catalyst immersed in 4 cm^3 of MO aqueous solution (10 mg·dm^{-3})	90% after 120 min (visible light)	—	[16]
TiO_2/CdS heterojunction (mixture)	0.63 mg·cm^{-3}of catalyst dispersed in MO aqueous solution (16 mg·dm^{-3}), 64 W fluorescent lamp	50% after 44 min, 100% after 120 min (UV light), $k_{app} = 2.14 \cdot 10^{-2}$ min^{-1}	2.39	this work
		50% after 225 min in (UV-vis light), $k_{app} = 3.1 \cdot 10^{-3}$ min^{-1}		

REFERENCES

[1] N. Serpone, E. Borgarello, M. Grätzel, J. Chem. Soc., Chem. Commun. **6**, 342-344 (1984).

[2] N. Serpone, P. Maruthamuthu, P. Pichat, E. Pelizzetti, H. Hidaka, J. Photochem. Photobio A **85**, 247-255 (1995).

[3] Y. Bessekhouad, N. Chaoui, M. Trzpit, N. Ghazzal, D. Robert, J.V. Weber, J. Photochem. Photobio. A **183**, 218-224 (2006).

[4] D. Robert, Catal. Today **122**, 20-26 (2007).

[5] Ch. Su, Ch. Shao, Y. Liu, J. Colloid Interf. Sci. **359**, 220-227 (2011).

[6] R. Daghrir, P. Drogui, D. Robert, Ind. Eng. Chem. Res. **52**, 3581-3599 (2013).

[7] G. Yang, B. Yang, T. Xiao, Z. Yan, Appl. Surf. Sci. **283**, 402-410 (2013).

[8] L. Liua, J. Lva, G. Xua, Y. Wanga, K. Xiea, Z. Chenc, Y. Wu, J. Solid State Chem. **208**, 27-34 (2013).

[9] F.-X. Xiao, J. Miao, H.-Y. Wang, B. Liu, J. Mater. Chem. **1**, 12229-12238 (2013).

[10] L. Lia, L. Wanga, T. Hub, W. Zhanga, X. Zhanga, X. Chen, J. Solid State Chem. **218**, 81-89 (2014).

[11] H. Zhu, R. Jiang, L. Xiao, L. Liu, C. Cao, G. Zeng, Appl. Surf. Sci. **273**, 661-669 (2013).

[12] X. Guoa, C. Chenc, W. Songa, X. Wanga, W. Dia, W. Qin, J. Mol. Catal. A-Chem. **387**, 1-6 (2014).

[13] D. Jiang, T. Zhou, Q. Sun, Y. Yu, G. Shi, L. Jin, Chin. J. Chem. **29,** 2505-2510 (2011).

[14] Y. Zhu, R. Wang, W. Zhang, H. Ge, X. Wang, L. Li, Mater. Res. Bull. **61**, 400-403 (2014).
[15] W. Chengyu., S. Huamei, T. Ying, Y. Tongsuo, Z. Guowu, Sep. Purif. Technol. **32**, 357-362 (2003).
[16] X. Zhou, F. Yang, B. Jin, L. Chen, S. Li, J. Nanomater., Article ID 678505 7 pages (2014).
[17] S. Feng, J. Yang, M. Liu, H. Zhu, J. Zhang, G. Li, Electrochim. Acta **83**, 321-326 (2012).
[18] G. Wu, M. Tian, A. Chen, J. Photochem. Photobio. A **233**, 65-71 (2012).
[19] H. Yao, W. Fu, H. Yang, J. Ma, M. Sun, Y. Chen, W. Zhang, D. Wu, P. Lv, M. Li, Electrochim. Acta **125**, 258-265 (2014).
[20] A. Trenczek-Zajac, A. Kusior, A. Lacz, M. Radecka, K. Zakrzewska, Mater. Res. Bull. **60,** 28-37 (2014).
[21] M. Xia, F. Wang, Y. Wang, A. Pan, B. Zou, Q. Zhang, Y. Wang, Mater. Lett. **64**, 1688-1690 (2010).
[22] S. Yang, A.S. Nair, S. Ramakrishna, Mater. Lett. **116**, 345-348 (2014).
[23] Y. Ma, X. Wang, Y. Jia, X. Chen, H. Han, C. Li, Chem. Rev. **114**, 9987-10043 (2014).
[24] M. Fujii, K. Nagasuna, M. Fujishima, T. Akita, H. Tada, J. Phys. Chem. C **113**, 16711-16716 (2009).
[25] M. Alexandre, P. Dubois, Mat. Sci. Eng. R. **28,** 1-63 (2000).
[26] https://www.aerosil.com/product/aerosil/Documents/TI-1243-Titanium-Dioxide-as-Photocatalyst-EN.pdf.
[27] C.A. Schneider, W.S. Rasband, K.W. Eliceiri, Nat. Methods **9**, 671-675 (2012)
[28] P. Scherrer, Abh. Kön Gesell. Wiss. Götting. **2,** 98-100 (1918).
[29] R.J. White, V.L. Budarin, J.H. Clark, Colloid. Surface. A **444**, 69-75 (2014).
[30] A.B. Murphy, Sol. Energ. Mater. **91**, 1326-1337 (2007).
[31] J. Kaur, S. Bansal, S. Singhal, Physica B **416**, 33-38 (2013).
[32] K. Dai, L. Lu, G. Dawson, J. Mater. Eng. Perform. **22**, 1035-1040 (2013).